LAWRENCE
LIVERMORE
NATIONAL
LABORATORY

LLNL-JRNL-673678

Impact of laser-contaminant interaction on the performance of the protective capping layer of 1w; high reflective mirror coatings

S. R. Qiu, M. A. Norton, R. N. Raman, A. M. Rubenchik, C. D. Boley, A. Rigatti, P. B. Mirkarimi, C. J. Stolz, M. J. Matthews

June 22, 2015

Applied Optics

Disclaimer

This document was prepared as an account of work sponsored by an agency of the United States government. Neither the United States government nor Lawrence Livermore National Security, LLC, nor any of their employees makes any warranty, expressed or implied, or assumes any legal liability or responsibility for the accuracy, completeness, or usefulness of any information, apparatus, product, or process disclosed, or represents that its use would not infringe privately owned rights. Reference herein to any specific commercial product, process, or service by trade name, trademark, manufacturer, or otherwise does not necessarily constitute or imply its endorsement, recommendation, or favoring by the United States government or Lawrence Livermore National Security, LLC. The views and opinions of authors expressed herein do not necessarily state or reflect those of the United States government or Lawrence Livermore National Security, LLC, and shall not be used for advertising or product endorsement purposes.

Impact of laser-contaminant interaction on the performance of the protective capping layer of 1ω high reflective mirror coatings

S.R. Qiu[1,*], M.A. Norton[1], R.N. Raman[1], A.M. Rubenchik[1], C.D. Boley[1], A. Rigatti[2], P.B. Mirkarimi[1], C.J. Stolz[1], and M.J. Matthews[1]

[1]*Lawrence Livermore National Laboratory, 7000 East Avenue, Livermore, CA 94551*
[2]*Laboratory for Laser Energetics, University of Rochester, 250 E. River Rd., Rochester NY 14623*
**Corresponding author: qiu2@llnl.gov, Phone: (925) 422-1636 Fax: (925) 423-0792*

Abstract

High dielectric constant multilayer coatings are commonly used on high reflector mirrors for high-peak-power laser systems, because of their high laser damage resistance. However, surface contaminants often lead to damage upon laser exposure thus limiting mirror lifetime and performance. One plausible approach to improve mirror overall resistance against laser damage, including that induced by laser-contaminant coupling, is to coat the multilayers with a thin protective capping (absentee) layer on top of the multilayer coatings. An understanding of the underlying mechanism by which laser-particle interaction leads to capping layer damage is important for the rational design and selection of capping materials of high reflective multilayer coatings. In this paper, we examine the responses of two candidate capping layer materials made of SiO_2 and Al_2O_3, respectively, over silica-hafnia multilayer coatings. These are exposed to a single oblique shot of a 1053 nm laser beam (fluence ~ 10 J/cm^2, pulse length 14 ns), in the presence of Ti particles on the surface. We find that the two capping layers show markedly different responses to the laser-particle interaction. The Al_2O_3 cap layer exhibits severe damage, with the capping layer becoming completely delaminated at the particle locations. The SiO_2 capping layer, on the other hand, is only mildly modified by a shallow depression. Combining the observations with optical modeling and thermal/mechanical calculations, we argue that a high-temperature thermal field from plasma generated by the laser-particle interaction above a critical fluence is responsible for the surface modification at each capping layer. The great difference in damage behavior is mainly attributed to the large disparity in the thermal expansion coefficient of the two capping materials, with that of Al_2O_3 layer being about 15 times greater than that of SiO_2.

OCIS codes: (310.1515) Protective coatings, (140.3330) Laser damage, (350.5400) Plasmas

Introduction

High-dielectric constant multilayer high-reflector (HR) coatings are critical to the performance of high-peak-power laser systems such as the National Ignition Facility, Laser Megajoule, and OMEGA [1-3]. While multilayer coatings have been shown to provide large laser-damage resistance in these systems, their performance and lifetime is often limited by damage induced through coupling between the laser and contaminating particles that are inadvertently deposited on the surface [4]. Contaminants observed on these optics consist of both organic and inorganic materials include oil, polyester fibers, ceramics, metal/metal oxides and alloys. These are often generated from optical processing, handling, installation, or laser operations [5-7]. Early studies showed that the laser-induced damage to the reflective surface is strongly dependent on the contaminant type and size, and the laser fluence [8]. While metallic particles tend to create larger damage sites on the coatings, transparent particles lead to smaller pits that roughen the surface. Furthermore, for transparent optical components, these contaminant particles when interacting with the laser beam, can also create pits and damage sites on both input and exit surfaces [9-12]. The resulting surface modification subsequently may lead to beam modulations [10] which can result in further damage on optical components downstream.

A number of strategies have been implemented to improve the laser-induced damage threshold of multilayer coatings and to extend their performance lifetime. These include eliminating or reducing coating defects[13, 14], post-conditioning by gradually exposing coatings from low to high fluences [15], and replacing initiated sites with benign micro-machined features that are stable at or above the operating (or use) fluence [16, 17]. Alternatively, adding an absentee overcoat (or protective capping layer) above the original high-reflective mirror coatings has also been shown to improve the laser damage resistance [18-20], the degree to which depends on capping layer thickness. In fact, protective capping layers have also been adopted to extend the lifetime of multilayer mirrors in EULV applications [21]. This previous work has created opportunities for the performance-enhancing practice of interference coatings against contaminant-induced laser damage by the addition of a protective or cap layer above the original design. However, the underlying mechanism by which coupling between the laser and contaminant causes damage to the protective layer is still elusive. In order to facilitate effective

selection and design of capping material and to develop a practical solution for contaminant removal, a better understanding of the physical principles is desired.

In this work, we combine experimental testing with optical/thermal/mechanical modeling to investigate the response of a capping layer, under 45° oblique irradiation of single pulses of 1053 nm, p-polarized laser light (fluence ~10 J/cm^2, pulse length 14 ns), in the presence of contaminant particles on the multilayer coating surface. The representative metallic contaminants are spherically-shaped Ti particles. Ti particles in general can be generated in high power pulsed laser systems through laser ablation within beam dumps and subsequent deposition of condensed metal vapor on nearby optics. Two silica-hafnia multilayer coating samples with different cap layer and high reflectivity (>99.5%), fabricated by e-beam physical vapor deposition, were used. Silica-hafnia multilayers are commonly used for high-reflectors in high-peak-power laser systems which require high laser damage resistance [22, 23]. The resistance to laser-induced damage due to contaminants is compared for capping layer materials Al_2O_3 and the previously used SiO_2[19]. Al_2O_3 is a large bandgap material and has been shown to have high laser-damage resistance [24-26]. Recent studies have demonstrated that inclusion of layers of such material in silica-hafnia multilayer coatings can reduce the overall coating stress and, more importantly, enhance the multilayer coating laser damage threshold [23]. Therefore, a damage-resistant Al_2O_3 layer to modify laser-particle coupling may offer an additional option for enhancing the performance of multilayer coatings in high-peak-power laser systems.

We found that the damage response of the two different capping layers to the laser-particle interaction exhibited a great contrast. At oblique incidence, the high fluence single-shot exposure caused the Al_2O_3 capping layer to be heavily damaged at the Ti particle locations. The damage sites were a result of the mechanical breakdown and subsequent delamination of the capping layer. On the other hand, an identical exposure on the sample with a SiO_2 capping layer, led to only a mild modification with a shallow depression in the capping layer, where no breakdown or delamination was observed. Combining these observations with modelling analysis, we argue that the laser-Ti interaction at the coating surface generates plasma ejecting towards the incident beam, thus elevating the temperature of the capping layer at the particle locations and modifies the surface. The difference in laser damage behavior observed between

the two capping layers is mainly attributed to the large disparity in thermal expansion coefficients, with that of the Al_2O_3 being approximately 15 times greater than that of SiO_2. Modeling suggests that the combination of oblique incidence, a spherical particle, and a high reflective surface, can result in substantial damaged areas, as observed.

Experimental and Modelling Methods

Multilayer coatings deposition and X-ray diffraction characterization

Coating depositions were performed in a 54-in. or a 56-in. vacuum chamber equipped with quartz heater lamps, dual electron-beam guns, multi-point quartz crystal monitors, a planetary substrate rotation, and cryopumps. Granular SiO_2 was evaporated from a continuously rotating pan while Hf metal or Al_2O_3 granules were deposited from a stationary six-pocket electron-beam gun [27]. The chamber was back-filled with oxygen during deposition of the Hf layers in order to oxidize the vapor plume at the substrate, resulting in a thin film coating of HfO_2. An oxygen back-fill could also be utilized during the silica or alumina layers, but the starting materials are already oxides. The back-fill process parameter could be used to optimize thin-film stress if required [23, 28]. The high reflector (>99.5% R) coatings were designed for a 1053 nm center wavelength, 45 degree angle of incidence, p-polarization. The design utilized 35 quarter-wave layers of alternating hafnia and silica with a half-wave top layer overcoat (or capping) of either Al_2O_3 (thickness: 360 nm) or SiO_2 (thickness: 410 nm). X-ray diffraction (XRD) was performed on a Pan Alytical x-ray diffractometer in a standard $2\theta/\theta$ mode using Cu Kα at λ = 1.54 Å. The step size was 0.02 degrees, and a longer-than-usual counting time of 20 seconds per point was used to improve the signal-to-noise ratio and render peaks more clearly discernable.

Laser damage testing

A schematic of laser damage testing of a capping layer on HR coatings in the presence of Ti particles is shown in Figure 1. For consistency throughout the paper in all figures, the laser is always incident from the left. Prior to contaminant-induced laser damage testing, the surface of the two samples of different capping layer materials were first laser conditioned by ramping the fluence from 2.5 J/cm^2 to 13 J/cm^2 in steps of 0.1 J/cm^2 (1053 nm, 14 ns). Laser conditioned surfaces were then contaminated with evenly distributed Ti spheres (nominal 30 ± 16 μm in diameter, Goodfellow, USA) by sprinkling commercially available Ti powders with a well-

developed protocol. Each sample was placed vertically in the testing system with a beam incident angle of 45°. The surfaces, with the deposited Ti particles, were then exposed to a single shot of the laser pulse (p-polarized, 1053 nm, 14 ns) at an average fluence of 10 J/cm^2. The laser system used for these tests was a Nd: glass zig-zag slab amplifier phase-conjugated laser system capable of producing 25 J, 1053 nm wavelength, 12.5 ns FWHM pulse of near diffraction-limited beam quality, single shot to 2 Hz. All fluence values measured with a calibrated scientific grade camera at the plane of the sample are reported normal to the propagation direction. Typical contrast as imaged on the sample was ~26% in the central 70% of the beam area. The actual beam area on the substrate was ~0.5 cm^2 due to the 45° angle of incidence. Peak fluence within the beam was typically two times the average fluence. The repetition rate of the laser used during these tests is 0.3 Hz. An additional camera is used with the reflected light to image the surface and obtain the location of the particles in the beam. An online long working distance microscope is the 3rd camera used during laser irradiation. It has sufficient resolution to observe plasma generated during a laser shot. For the experiments reported here it was primarily used to identify possible damage during the conditioning shots prior to Ti application. A similar setup of the laser system can be found in Ref. [8].

Optical modeling

The fluence at the particle surface cannot be inferred immediately from the incident laser fluence, due to the important role of light reflected from the mirror. Since the size of the Ti particles is much larger than the laser wavelength, ray tracing is suitable for optical modeling. Interference effects are expected to be significant only in the vicinity of the point of contact with the mirror, where the intensity is low. To carry out the ray-tracing, we employed the commercial application FRED (distributed by Photon Engineering, LLC, Tucson, AZ), a multipurpose optics code widely used in optical design and analysis. We previously used this code in calculating laser interactions with composite materials [29] and metal powders [30]. Each ray travels from surface to surface, with a particular power in each polarization. At the surface of the particle, rays are absorbed and reflected according to the Fresnel absorptivity and reflectivity of Ti (index of refraction taken as n = 3.45 + 4 i). The absorbed power is noted, and only the reflected ray is followed. The absorptivity and reflectivity depend on both the angle of incidence and the polarization.

Optical and Electron Microscopy

Laser-exposed samples were characterized by high resolution optical (0.9 μm/pixel, Benchmark, View MicroMetrology), laser scanning confocal (638 nm, 0.8 NA, 10 nm axial resolution, VKX110, Keyence Corp.), and field emission scanning electron microscopies (FE-SEM, FEI XL 30S FEG) with EDS x-ray microanalysis (EDAX Brand, Co.) for particle distribution, damage morphology and topology, and chemical contents, respectively. Analysis of images from both online and offline with resolution ~ 12 microns per pixel microscopes also led to the assessment of damage probability of coatings with different cap layer composition due to the laser-Ti particle interaction. All SEM analysis samples were coated with a 10 nm layer of carbon to avoid surface charging during imaging.

Results

The structure of the capping layer was determined by comparing the XRD spectra collected from the SiO_2 and Al_2O_3 capped mirrors. It was found that the SiO_2 cap layer is crystalline containing mostly the α-quartz phase, while the Al_2O_3 cap is non-crystalline. Figure 2 depicts two superimposed XRD spectra from the two samples. The two spectra show nearly identical characteristics except at the 2θ of 26.1° where the SiO_2 curve exhibits an additional peak (see Figure 2b for details). This peak is close to that from the bulk α-quartz (101) plane which is nominally at 26.6°. Because thin films can often have shifted peaks due to stress and other factors [31], the observed peak represented a crystalline α-quartz phase within the SiO_2 capping layer. For the Al_2O_3 capping layer, the XRD spectrum showed no characteristics peaks from either the α-alumina (in the 25°-68° range, Figure 1a) or the β-alumina phase (in the 5°-11° 2θ range). Thus the Al_2O_3 capping layer was amorphous.

The Ti particles (see Figure 1a) that were sprinkled onto the capping layer surfaces were spherically shaped. While variations in size were inevitable, the majority of the particles on the surface were approximately 30 μm in diameter. The apparent larger particles were usually aggregates of smaller ones.

The presence of Ti spheres on the surface leads to coating modification upon laser exposure. Figure 3a shows the surface of a tested area of the Al_2O_3-capped sample after one shot of a laser beam at 45° off normal (from the left of the page) with an average fluence of 10 J/cm^2. While no

original particles remain on the surface after the exposure, the capping layer is heavily damaged subsequently, as displayed by the bright spots in Figure 3a. In general, the damaged sites exhibit a distorted oval shape with the major axis pointing along the horizontal direction. The size of these damage sites range from a few μm to approximately 400 μm along the longer dimension (see Location A). Nearly all of the damaged areas are associated with the particles on the surface prior to laser exposure. The correlation between the sites and the locations of the particles on the surface is marked by the red dots within the damage areas. Without exception, for all of the oval-shaped damage sites, the particles are situated near the right tip of the oval. Based on the confocal microscope analysis (Figure 3b), the damage sites have an approximate depth from the pristine layer ranging between 250 nm and 350 nm. Since the capping layer is ~360 nm thick, the result suggests that there may be partial to full removal of the capping materials surrounding the damage sites. A horizontal profile line-out through a damage site is inserted in Figure 3b to demonstrate the depth profile of a damaged site from the confocal microscope image.

A closer examination of damaged regions using SEM shows that the entire Al_2O_3 capping layer is removed from the layer below. Figure 4a is a representative region of modified areas (Location A) containing three adjacent damage sites where two overlap one another. At the circumference of each site, the edges are rough and show clear breakage from the host material (Figure 4b). Higher resolution images of the edges confirm that they are in fact only one layer thick (see Figure 4c for example). This indicates that the interaction between the laser and Ti particle on the coating surface leads to surface modification by delaminating the capping layer. Moreover, within nearly all the damage sites, there remains a pocket or island of Al_2O_3 capping material that is not damaged (next to the red dots in Figure 4a). Interestingly, this undamaged pocket is always close to the location of the Ti particle prior to the exposure. This observation suggests that, behind the particle, there may be a “low energy” spot where the particle provides a protecting shadow for the capping layer situated there.

Elemental mapping of EDX at the vicinity of the damaged areas shows detectable Ti on the surface. The presence of Ti is usually associated with apparent trail-like structures pointing toward the right side of the surface when observed in both optical and low resolution SEM microscopes. An example of such features is shown in area A1 of Figure 4a. A close-up view of

this region shows very interesting characteristics. First there are a number of droplet-like Ti particles on the surface. These particulates all have smooth surfaces suggesting that they have been in a molten state before landing on the surface. Second, some of these particulates are aligned along a straight line in a particulate direction indicating their trajectory. Furthermore, some of the particulates create secondary modification to the capping surface along their pathways. Examples are shown in areas of A2 and A3. The imprints shown in both A2 and A3 suggest that molten particles landed in this area while they were still at a relatively high temperature. The heat released from the particle and coupled into the capping layer can lead to mechanical strain in the film due to thermal expansion. This explains the trace of Ti left at the edge of the modified area.

In marked contrast to that of the Al_2O_3 capping, the presence of the Ti particle on the SiO_2 capping layer resulted in much less modification to the surface after exposure to one shot of the laser beam with identical conditions (fluence, polarization, pulse length, and angle of incidence). Instead of a complete delamination, the modified areas on the SiO_2 surface show no removal of the capping material. The first layer remains intact though modified. Figure 5a shows a micrograph of the laser-modified areas on the SiO_2 capping surface. Similar to that with the Al_2O_3 capping layer, each damage site is clearly associated with the presence of one or more Ti particles in the vicinity. Confocal microscope depth profiling (Figure 5b) corresponding to Figure 5a indicates that the modification is caused by depression of the capping materials, and the depth of the depression is about 150 nm.

A closer examination of the modified areas at different length scales using SEM indicates that there is no material breakdown or removal; instead the SiO_2 capping layer is slight depressed at the Ti particle locations. However, other additional characteristics are very similar to those observed on the Al_2O_3 capping layer surface. First, each of the modified sites exhibits an oval shape with similar distortion (Figures 6a). Next, splash-like features pointing toward the right side of the image are associated with each site (Figure 6b), and the beginning of the trace is closely related to the location of the Ti particles before exposure. Furthermore, the trail-like features are the modified area of the SiO_2 surface by the travelling molten Ti particulates (Figure 6c).

Figure 7 depicts the relationship between the incident local fluence (ϕ) and the probability (P) that the coatings will damage at the location of a Ti particle after one shot (mean ± standard deviation of corresponding binomial distribution, typically 10 particles per fluence bin). Damage is designated as any visible change in the image of the capping surface obtained using the offline optical microscope described above. Damage probability was calculated as the fraction of particles that damaged the coating surface after one laser shot. While the pits on the alumina-coated sample were much deeper than that of the silica-coated sample, the probability at which a Ti particle leads to damage was fairly similar on both capping layers. For silica film the onset of damage appears to occur at slightly lower fluence (at 50% damage probability, $\phi_{SiO2} = 2.5$ vs. $\phi_{Al2O3} = 4.0$ J/cm^2), suggesting that this coating is more likely to damage at lower fluence even though the damage is shallower.

Discussion

Exposure of laser light on metal particles can lead to metal heating and evaporation at the surface when the laser fluence is sufficiently high. Subsequently, interactions between the metal vapor and laser light result in ionization and plasma formation. In the current system, because of the reflective coatings beneath the Ti particles and the oblique incidence of the incoming laser, the light intensity on the metal surface becomes the sum of that directly impinged and that reflected from the mirror. As a result, the plasma formation threshold of the Ti particle on the mirror surface will be lower than that on top of transparent optics. Following laser absorption, hot plasma develops, the temperature of the mirror surface rises, leading to material evaporation of surface layers. The disparity in thermal expansion coefficients can induce stresses between two adjacent layers, especially the capping layer and the layer below [19]. When sufficiently large, this stress can lead to modification or even delamination of the top coating layers. This also holds when only the top layer is heated during the pulse, which is discussed below. We were not able to measure the intrinsic stress of the films but would note that because temperatures on the order of thousands of degrees are realized, the stress arising from significant thermal expansion coefficient differences will be significantly larger than the expected intrinsic stress for the films. In addition, the recoil momentum from the ejected plasma propels the partially melted contaminant along the surface, creating additional damage along its trajectory. This successive

chain of events after the laser shot is responsible for the reported observations. The underlying mechanism is discussed below in detail.

The onset of the evaporation process takes place when the deposited energy per unit area in the outer layer of the particle reaches a value of about $H(D\tau)^{1/2}$, where H is the enthalpy per unit volume required to evaporate the material, τ is the laser pulse duration and D is the thermal diffusion constant. Typically, the ablation threshold is close to the plasma formation threshold. Assuming a flat surface, the threshold fluence ϕ_t is obtained from energy balance via $\phi_t = H(D\tau)^{1/2}/A$, where A is the metal absorptivity. For the Ti particle considered in this paper, we have H ~ 47.3 kJ/cm^3 (thermal energy plus evaporation enthalpy), D ~ 0.1 cm^2/s, and A ~ 0.4. Thus the threshold fluence of a 14-ns pulse is ϕ_t ~ 3.7 J/cm^2.

The distribution of the absorbed intensity over the spherical particle surface, obtained through simulations with FRED, is shown in Figure 8a. Because of reflections from the mirror, the peak absorbed intensity occurs at an angle of about 80° from the top of the particle, instead of 45°, without the mirror (see Figure 8b). In the presence of the mirror, the total power absorbed by the sphere is increased by 81% and the maximum local absorbed intensity is increased by about 26% (of course shifting from 45° to 80°). Recall that the overall expanse of absorption is increased by the mirror. Thus in the presence of the reflective or mirror surface, it is sufficient to have only 2.9 J/cm^2 (instead of 3.7 J/cm^2) in the incident beam in order to generate plasma from the Ti particles.

The ejection of vaporized material or plasma from the Ti surface can lead to a transfer of momentum, resulting in recoil movement of the particle itself. Because the maximum absorbed intensity is located at only 10° above the particle equator, we expect that the remnants of the particle to recoil along or near the coating surface. A method of calculating the shaped particle momentum was developed by Liedahl *et al.* [32]. For a given infinitesimal element of the surface, the acquired momentum dP is proportional to the incident fluence $d\phi$ and is directed along the normal to the surface, according to $dP = C_m\, d\phi$. The coupling coefficient C_m has been measured for a number of materials and laser parameters [33]. For fluences that are not too far from the ablation threshold, the coupling coefficient is constant [32, 33]. By integrating over the surface of the particle, the magnitude and the direction of the received momentum can be determined. When the calculation is applied to this case, it is found that the recoil momentum is

directed at an angle of 10° below the horizontal direction away from the beam side. Thus the heating particle is expected to move toward the right along the capping layer surface, agreeing well with experimental observation.

When the ablated hot materials strike the surface they can heat up the capping layer. The local heating near the contaminant particle induces stresses in the capping layer and multilayer coatings, due to the difference in the thermal expansion coefficients. If the induced stresses are sufficiently high, they can cause breakage and delamination. For purpose of estimate, we will use stresses calculated in the static limit. This means that the results will be reliable close to the point of heating. In terms of elasticity, the capping layer and HR coatings can be considered as thin plates. Now during the laser pulse, the heat diffuses a distance of order $(D_c\ \tau)^{1/2}$, in terms of an approximate thermal diffusion constant D_c, which is of order 0.01 cm^2/s. Thus the diffusion length is of order 100 nm, which is comfortably less than the capping layer thickness of 360-410 nm. As an estimate, therefore, it is reasonable to assume that only the capping layer is heated by the plasma. In this case, the top coating layer (HfO_2) can be viewed as a substrate, and the stress induced in the capping layer is given by [32]

$$\sigma_c = -\frac{E_c}{1-\nu_c}\alpha_c \Delta T$$

where E_c is the Young modulus of the capping layer, ν_c is its Poisson ratio, α_c is its thermal expansion, and ΔT is the temperature excursion from ambient. The stress is transverse.

Using the mechanical data provided in Table 1, we find that the absolute value of the stress induced in the Al_2O_3 cap is approximately 64 times greater than that induced in the SiO_2 cap. This explains the much greater damage in the Al_2O_3 layer, including delamination from the layer below. Incidentally, if the heat had been assumed to penetrate through the HfO_2 layer, then in the equation above the thermal expansion coefficient α_c would have been replaced by $\alpha_c - \alpha(HfO_2)$. In this case, the absolute value of the ratio of the stresses in Al_2O_3 and SiO_2 would have decreased to about 6. This seems too small in view of the observed difference in damage, confirming our assumptions.

We now show that the experimental phenomena observed in Figures 4-6 are consistent with the above discussion. Briefly, the off-normal impinging laser beam strikes both the spherical

particle and the reflective surface, leading to an intensified absorption on the particle at about 80° from the vertical (shifted from 45°), as seen in Figures 8 and 9a. The expanding plasma is ejected almost horizontally beneath the incoming beam (centered at ~10° from the horizontal surface) and burns a large oval-shaped area of the capping layer within the vicinity of the particles (Figure 9b). The response of the capping materials to the plasma-generated thermal field is directly related to their thermal-mechanical properties including the thermal expansion coefficient (Table 1). Due to the transient nature of the pulse, only the capping layer is affected by the thermal field. Because of its large thermal expansion, the Al_2O_3 layer is subject to large mechanical distortion under the thermal field which can lead to severe damage and delamination from the layer below. The SiO_2 capping layer, on the other hand, responds with only mild modification.

At the same time, the recoil momentum that the partially melted particle receives from the ejected plasma is nearly parallel to the mirror surface and thus carries the particle along the surface in the opposite direction toward the right, in Figure 9b). This motion causes further damage/modification to the capping layer surface, and it leaves molten droplets on the substrate.

It is important to note that these phenomena are expected to be highly sensitive to the particle shape. For a relatively flat particle attached to the surface (consistent with mechanically-abraded material), the ablated plasma is directed almost normal to the surface and is expected to produce less delamination and smaller damage area than that from a spherical particle. Lateral motion is possible due only to absorption along the edge. Hence the extent of damage is expected to decrease for flatter particles.

Conclusion

In summary, laser damage testing at oblique incidence shows that laser-contaminant interaction on HR multilayer coatings leads to damage to a surface the capping. Oblique incidence along with a reflective surface leads to intensification of the absorbed light on the Ti particles. Under the identical laser irradiation conditions, damage on the Al_2O_3 capping layer is much more severe than that on the SiO_2 layer; at the Ti particle locations, the Al_2O_3 capping layer is completed delaminated but the SiO_2 layer is only mild modified. The large difference in damage behavior is mainly attributed to the disparity in the thermal expansion coefficients of the two capping materials, with that of the Al_2O_3 layer being about 15 times greater than that of SiO_2.

Thermal-mechanical calculations combined with optical modeling show that the large difference in thermal expansion coefficients leads to a large differences in thermally induced mechanical stress between the capping layer and the adjacent layer below. In the Al_2O_3 case, this is approximately 64 times greater than in the SiO_2 case. The large thermal-mechanical stress is responsible for the detachment of the Al_2O_3 capping layer from the adjacent HfO_2 layer below. Thus SiO_2 is shown to be a more effective material for use as a capping material to protect against debris-induced laser ablation and damage on high power dielectric coating mirrors.

Acknowledgements

This work was performed under the auspices of the U.S. Department of Energy by Lawrence Livermore National Laboratory under Contract DE-AC52-07NA27344 and funded through Laboratory Directed Research and Development Grant 14-ERD-098. We would like to thank Mr. Edwin Sedillo for collecting the SEM images and the EDX measurements, Gabe Guss, John Adams, and Raluca Negres for making fiducials and William G. Hollingsworth for performing the laser damage testing and optical microscope imaging. (LLNL-JRNL-673678)

References

1. C. J. Stolz, "Status of NIF mirror technologies for completion of the NIF facility," in 2008), 710115-710115-710111.
2. B. Pinot, H. Leplan, F. Houbre, E. Lavastre, J.-C. Poncetta, and G. Chabassier, "Laser megajoule 1.06-µm mirror production with very high laser damage threshold," in 2002), 234-241.
3. J. B. Oliver, A. L. Rigatti, J. D. Howe, J. Keck, J. Szczepanski, A. W. Schmid, S. Papernov, A. Kozlov, and T. Z. Kosc, "Thin-film polarizers for the OMEGA EP laser system," in 2005), 599119-599119-599118.
4. S. Palmier, S. Garcia, and J.-L. Rullier, "Method to characterize superficial particulate pollution and to evaluate its impact on optical components under a high power laser," OPTICE **47**, 084203-084203-084207 (2008).
5. T. Jitsuno, H. Murakami, K. Kato, E. Sato, K. Mikami, S. Motokoshi, N. Miyanaga, and H. Azechi, "Recent progresses on insights of laser damage mechanisms and influence of contamination in optics," in 2013), 87860B-87860B-87866.
6. W. H. Gourdin, E. G. Dzenitis, D. A. Martin, K. Listiyo, G. A. Sherman, W. H. Kent, R. K. Butlin, C. J. Stolz, and J. A. Pryatel, "Insitu surface debris inspection and removal system for upward-facing transport mirrors of the National Ignition Facility," in 2005), 107-119.
7. X. L. Ling, G. Wang, Y. N. Zhao, X. F. Liu, and J. D. Shao, "Laser-induced damage of the optical coatings due to organic contamination in vacuum," Applied Surface Science **270**, 346-351 (2013).
8. M. A. Norton, C. J. Stolz, E. E. Donohue, W. G. Hollingsworth, K. Listiyo, J. A. Pryatel, and R. P. Hackel, "Impact of contaminates on the laser damage threshold of 1ω HR coatings," in 2005), 59910O-59910O-59919.
9. S. Palmier, J. Luc Rullier, J. Capoulade, and J. Yves Natoli, "Effect of laser irradiation on silica substrate contaminated by aluminum particles," Appl. Optics **47**, 1164-1170 (2008).
10. M. J. Matthews, N. Shen, J. Honig, J. D. Bude, and A. M. Rubenchik, "Phase modulation and morphological evolution associated with surface-bound particle ablation," J. Opt. Soc. Am. B-Opt. Phys. **30**, 3233-3242 (2013).
11. J. Honig, M. A. Norton, W. G. Hollingsworth, E. E. Donohue, and M. A. Johnson, "Experimental study of 351-nm and 527-nm laser-initiated surface damage on fused silica surfaces due to typical contaminants," in *Proc. SPIE 5647, Laser-Induced Damage in Optical Materials*, 2005), 129-135.
12. F. Y. Genin, M. D. Feit, M. R. Kozlowski, A. M. Rubenchik, A. Salleo, and J. Yoshiyama, "Rear-surface laser damage on 355-nm silica optics owing to Fresnel diffraction on front-surface contamination particles," Appl. Optics **39**, 3654-3663 (2000).
13. C. J. Stolz, J. E. Wolfe, P. B. Mirkarimi, J. A. Folta, J. J. Adams, M. G. Menor, N. E. Teslich, R. Soufli, C. S. Menoni, and D. Patel, "Substrate and coating defect planarization strategies for high-laser-fluence multilayer mirrors," Thin Solid Films.
14. R. Chow, S. Falabella, G. E. Loomis, F. Rainer, C. J. Stolz, and M. R. Kozlowski, "Reactive evaporation of low-defect density hafnia," Appl. Optics **32**, 5567-5574 (1993).
15. A. B. Papandrew, C. J. Stolz, Z. Wu, G. E. Loomis, and S. Falabella, "Laser conditioning characterization and damage threshold prediction of hafnia/silica multilayer mirrors by photothermal microscopy," in 2001), 53-61.
16. S. R. Qiu, J. E. Wolfe, A. M. Monterrosa, M. D. Feit, T. V. Pistor, and C. J. Stolz, "Searching for optimal mitigation geometries for laser-resistant multilayer high-reflector coatings," Appl. Optics **50**, C373-C381 (2011).

17. J. E. Wolfe, S. R. Qiu, C. J. Stolz, M. Thomas, C. Martinez, and A. Ozkan, "Laser damage resistant pits in dielectric coatings created by femtosecond laser machining," Proc. SPIE **7504**, 750405 (2009).
18. C. K. Carniglia, J. H. Apfel, T. H. Allen, T. A. Tuttle, W. H. Lowdermilk, D.Milarn, and F. Rainer, "Recent damage results on silica/titania reflectors at 1 micron," NBS Special Pub. **568**(1979).
19. C. C. Walton, F. Y. Genin, R. Chow, M. R. Kozlowski, G. E. Loomis, and E. L. Pierce, "Effect of silica overlayers on laser damage of HfO2-SiO2 56 degrees incidence high reflectors," in 1996), 550-559.
20. Z. Wu, Z. Fan, and Z. Wang, "Damage Threshold Dependence on Film Thickness," NIST Special Pub. **775**(1988).
21. S. Bajt, N. V. Edwards, and T. E. Madey, "Properties of ultrathin films appropriate for optics capping layers exposed to high energy photon irradiation," Surface Science Reports **63**, 73-99 (2008).
22. C. J. Stolz, M. D. Thomas, and A. J. Griffin, "BDS thin film damage competition," in 2008, 71320C-71320C-71327.
23. J. B. Oliver, P. Kupinski, A. L. Rigatti, A. W. Schmid, J. C. Lambropoulos, S. Papernov, A. Kozlov, C. Smith, and R. D. Hand, "Stress compensation in hafnia/silica optical coatings by inclusion of alumina layers," Opt. Express **20**, 16596-16610 (2012).
24. M. Zhu, K. Yi, D. Li, H. Qi, Y. Zhao, J. Liu, X. Liu, G. Hu, and J. Shao, "Study on the laser-induced damage performance of HfO_2, Sc_2O_3, Y_2O_3, Al_2O_3 and SiO_2 monolayer coatings," in 2013, 888508-888508-888508.
25. M. Henyk, D. Wolfframm, and J. Reif, "Ultra short laser pulse induced charged particle emission from wide bandgap crystals," Applied Surface Science **168**, 263-266 (2000).
26. M. Reichling, A. Bodemann, and N. Kaiser, "Defect induced laser damage in oxide multilayer coatings for 248 nm," Thin Solid Films **320**, 264-279 (1998).
27. J. H. J. B. Oliver, A. Rigatti, D. J. Smith, and C. Stolz, "High precision coating technology for large aperture NIF optics," Optical Interference Coatings, OSA Technical Digest (Optical Society of America, Washington, DC, ThD2 (2001).
28. D. J. S. J. F. Anzellotti, R. J. Sczupak, and Z. R. Chrzan, "Stress and environmental shift characteristics of HfO2/SiO2 multilayer coatings,," in *Laser-Induced Damage in Optical Materials*, (SPIE, Bellingham, WA, 1996), 258-264.
29. C. D. Boley and A. M. Rubenchik, "Modeling of laser interactions with composite materials," Appl. Optics **52**, 3329-3337 (2013).
30. C. D. Boley, S. A. Khairallah, and A. M. Rubenchik, "Calculation of laser absorption by metal powders in additive manufacturing," Appl. Optics **54**, 2477-2482 (2015).
31. B. D. Cullity, *Elements of X-ray Diffraction* (Addison-Wesley, Reading, Massachusetts 1978).
32. D. A. Liedahl, A. Rubenchik, S. B. Libby, S. Nikolaev, and C. R. Phipps, "Pulsed laser interactions with space debris: target shape effects," Advances in Space Research **52**(2013).
33. J. C. R. Phipps, T. P. Turner, R. F. Harrison, G. W. York, W. Z. Osborne, and X. F. C. G. K. Anderson, L. C. Haynes, H. S. Steele and K. C. Spicochi, "Impulse coupling to targets in vacuum by KrF, HF, and CO2 single-pulse lasers," J. Appl. Phys. **64**(1988).

Figure 1: Schematics of testing damage induced by laser-particle interaction on highly reflective dielectric multilayer coatings, with different cap layers.

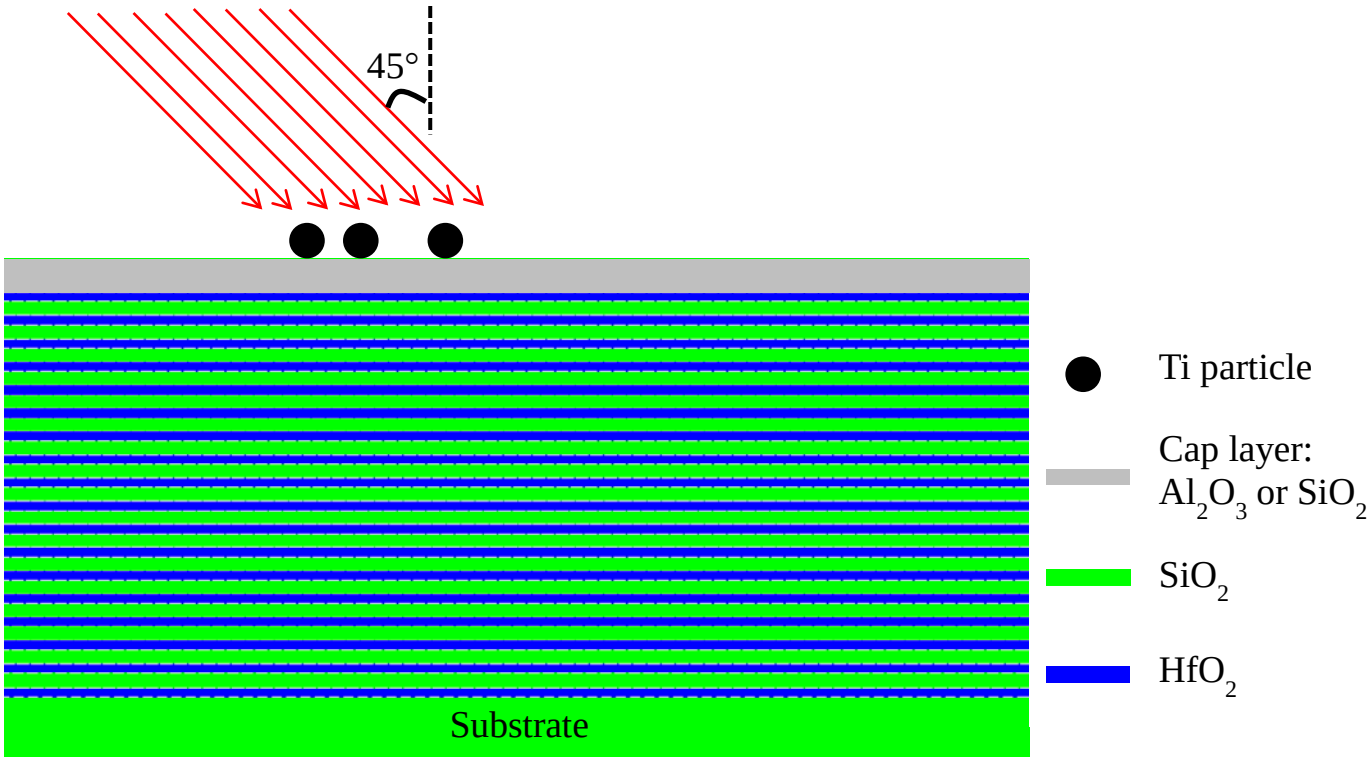

Figure 2: Superimposed XRD spectra collected from multilayers with SiO_2 (blue line) and Al_2O_3 (red line) cap layer, respectively, showing that the SiO_2 cap layer is crystalline and the Al_2O_3 cap layer is amorphous. (a) Scans at the 2θ angle range between 10° and 90°. (b) A close-up comparison of the two spectra between 20° and 30°.

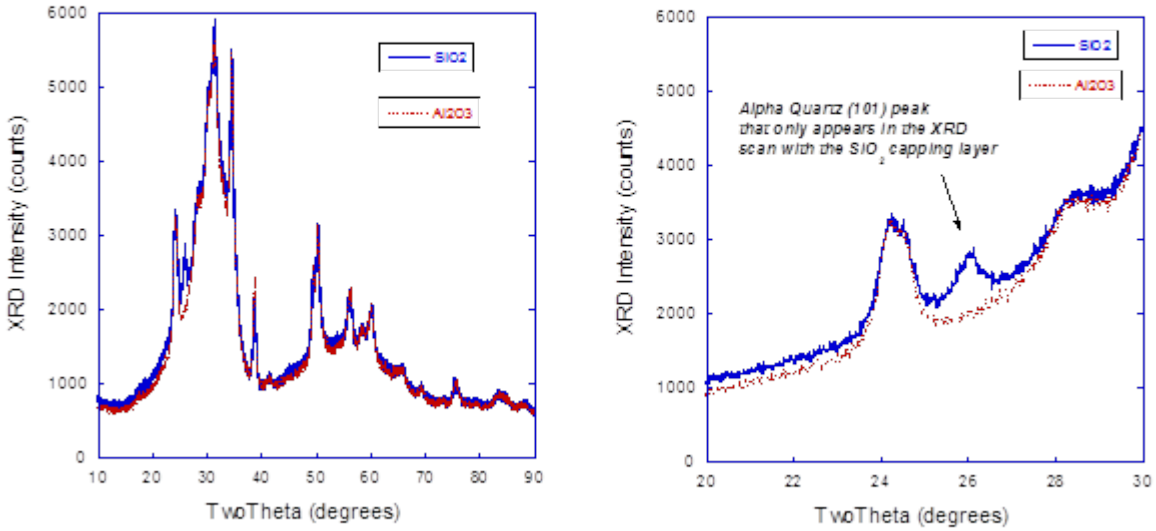

Figure 3: Optical images of damage sites on multilayer coating with the Al_2O_3 cap layer. (a) Overlay of damage site after one laser shot at ~ 10 J/cm^2 with Ti particle locations (red dots). The insert is the SEM image of a typical Ti particle (25 μm in diameter) used in the damage testing. (b) Confocal microscope image revealing the depth map of the damage sites following one laser shot. Inset: horizontal line-out profile of indicated pit.

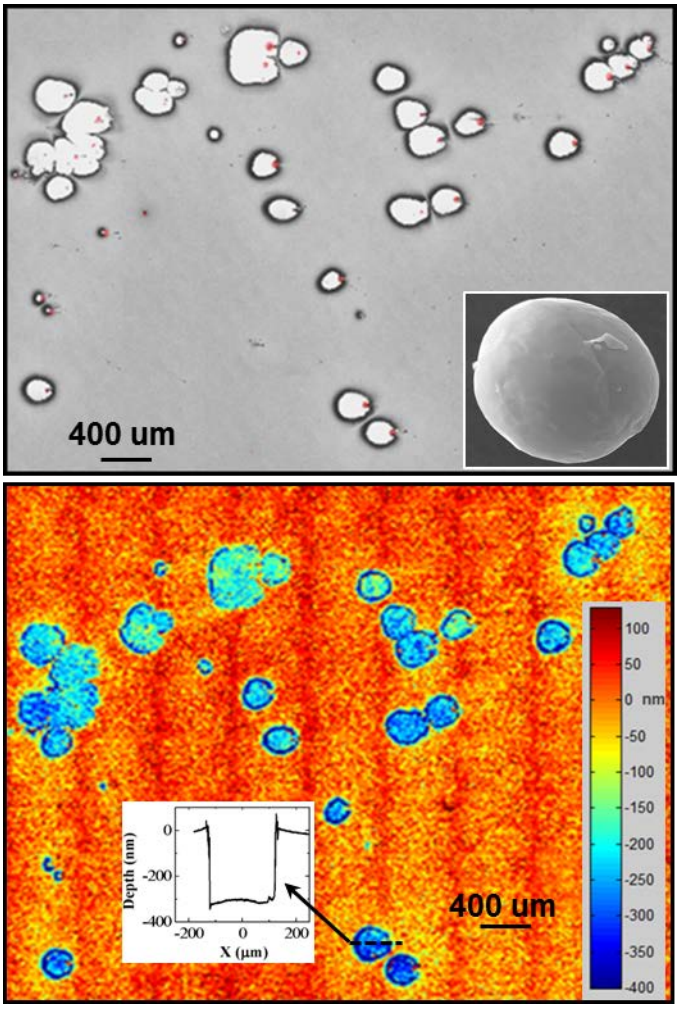

Figure 4: SEM images showing the morphology of damage site in location A at different resolutions. (a) The insert is the optical image of location A. (b) A close-up view of the area also shows the remaining pieces that are close to the particle location (next to the red dots). (c) High resolution image shows the delamination of the top layer. Image was collected at a rotated 180° with respect to others. (d) A close-up view of area A1 shown in (a). Arrows show molten Ti droplets on the surface.

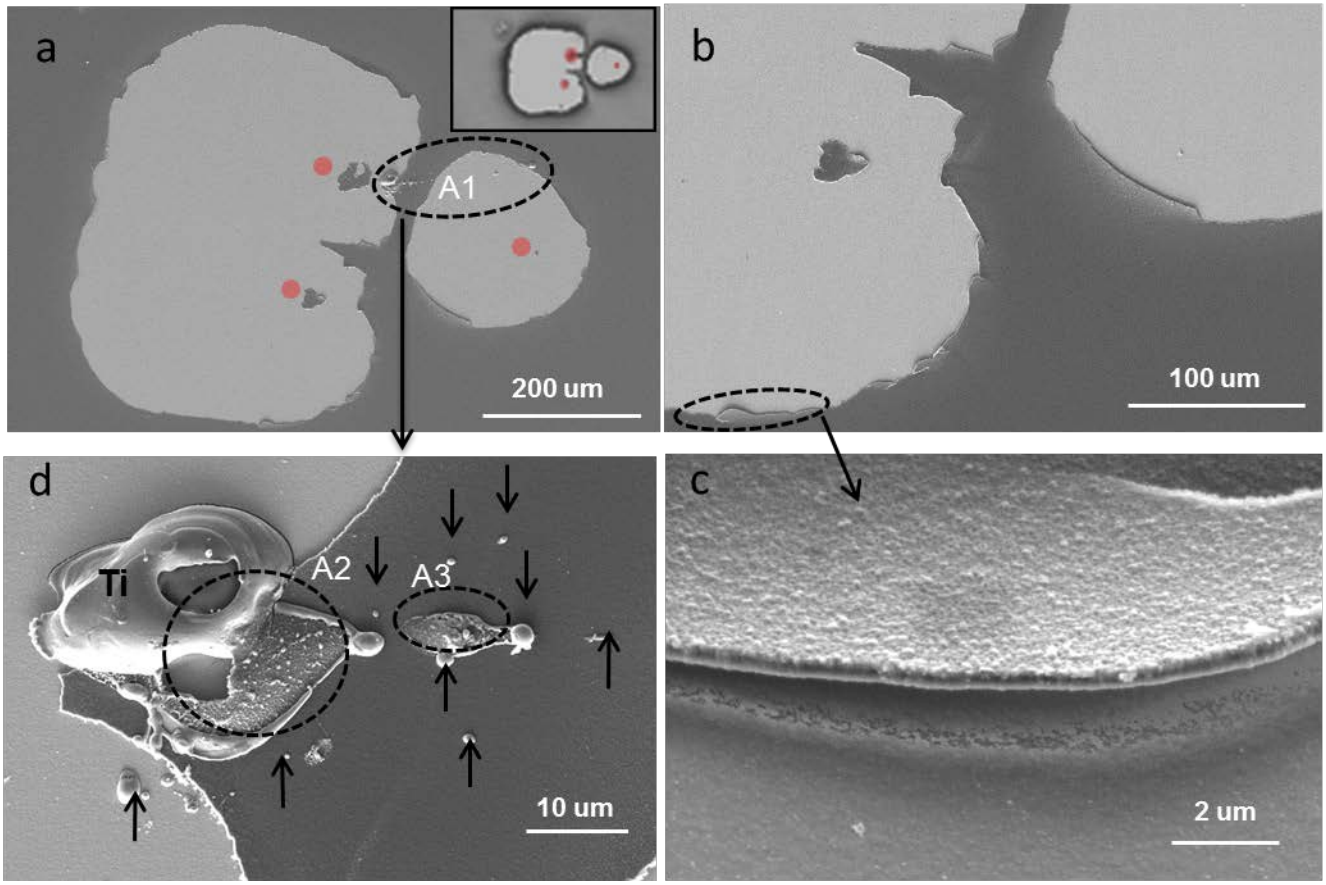

Figure 5: Optical images of modified sites on multilayer coating with the SiO_2 cap layer. (a) Overlay of modified site after one laser shot at ~ 10 J/cm^2 with Ti particle locations (red dots). (b) Confocal microscope image revealing the depth map of the modified site following one laser shot.

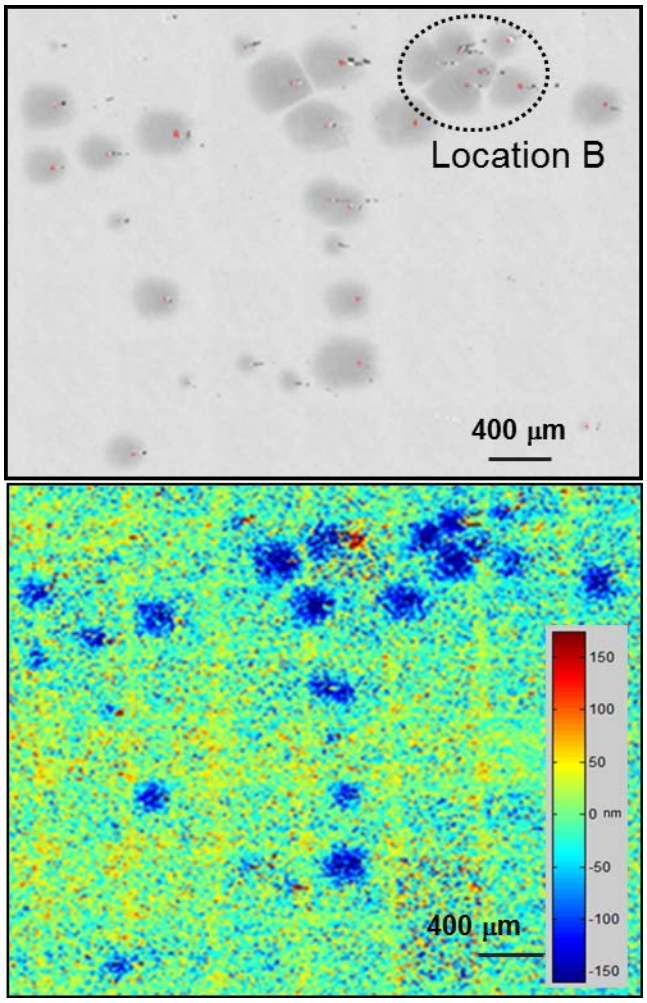

Figure 6: SEM images showing the modified areas on the SiO_2 capping layer after one laser shot. (a) Low resolution image containing several modified sites. The insert is the optical image at location B with the red dots indicating particle locations prior to laser shot. (b) A close-up view of location B. Within the modified area which represented by the polygon regions, there are directional trail-like features associated with each of them. (c) A higher resolution view of location C showing trail-like feature.

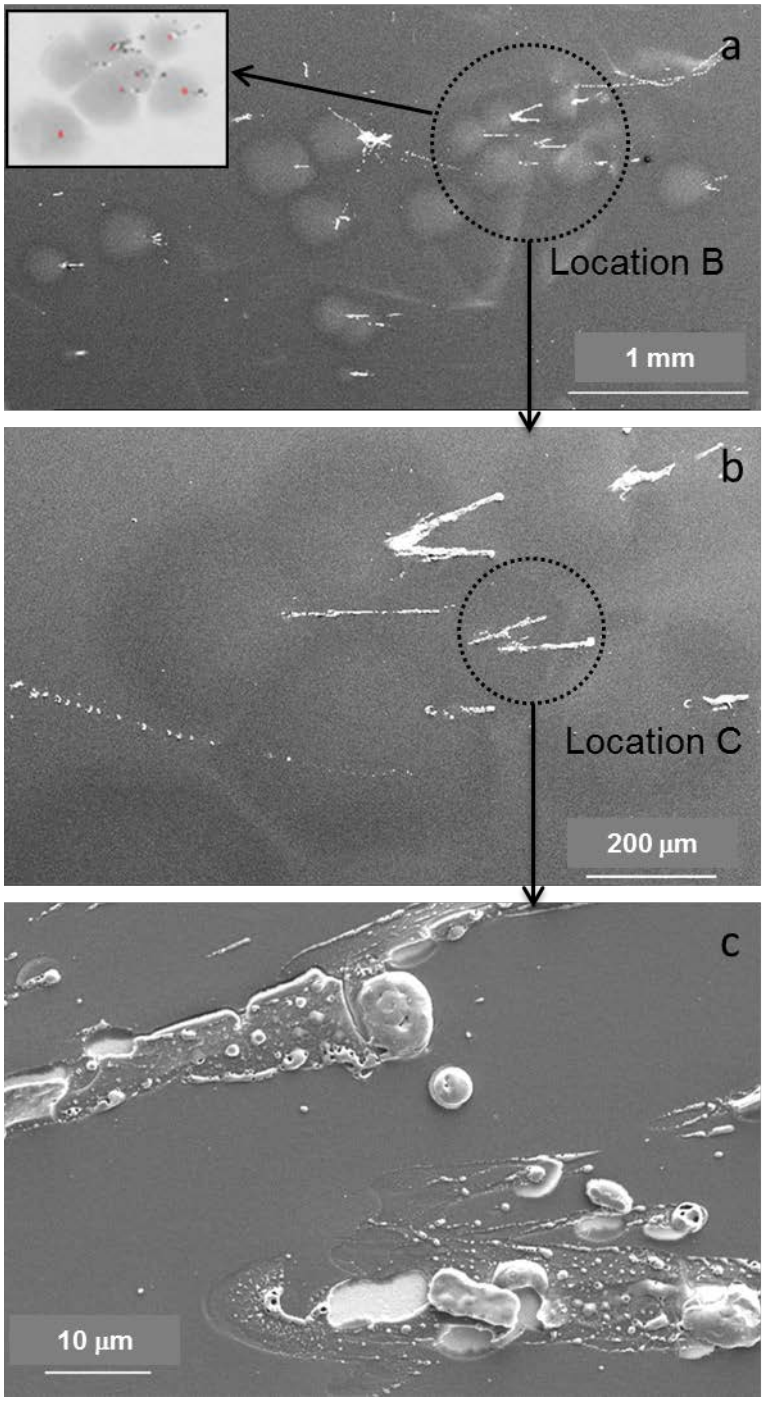

Figure 7: Fluence dependence of the damage probability of HR mirror coating surface with two different protective cap layers at the location of Ti particles. Error bars represent the standard deviation of the corresponding binomial distribution for each fluence bin.

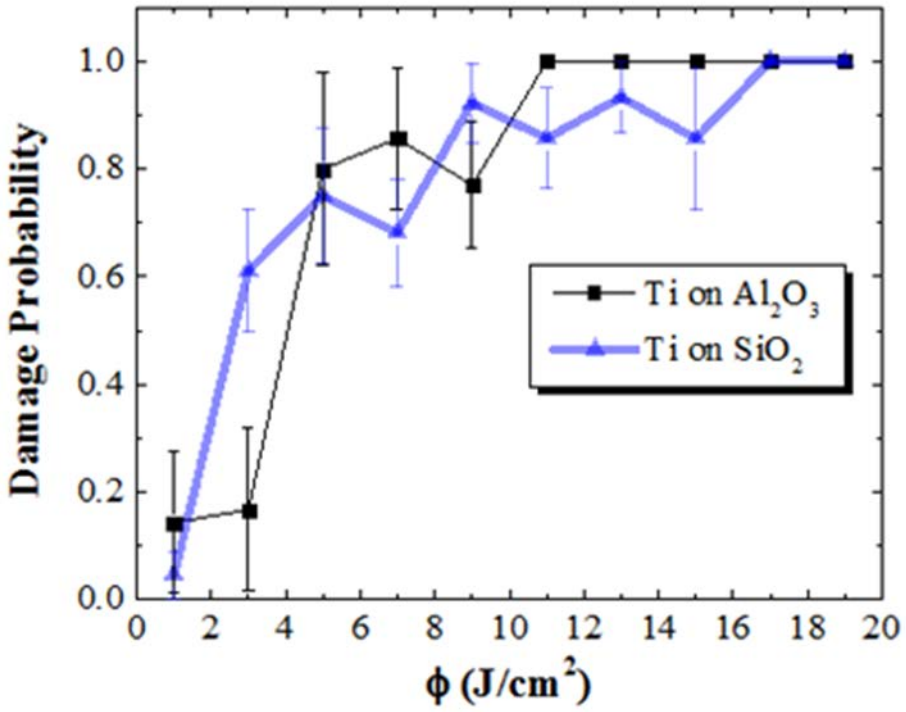

Figure 8: (a) Absorbed intensity, normalized by the maximum value. The splotches at the front should be ignored. (b) Absorbed intensity in the absence of the mirror (same color scale).

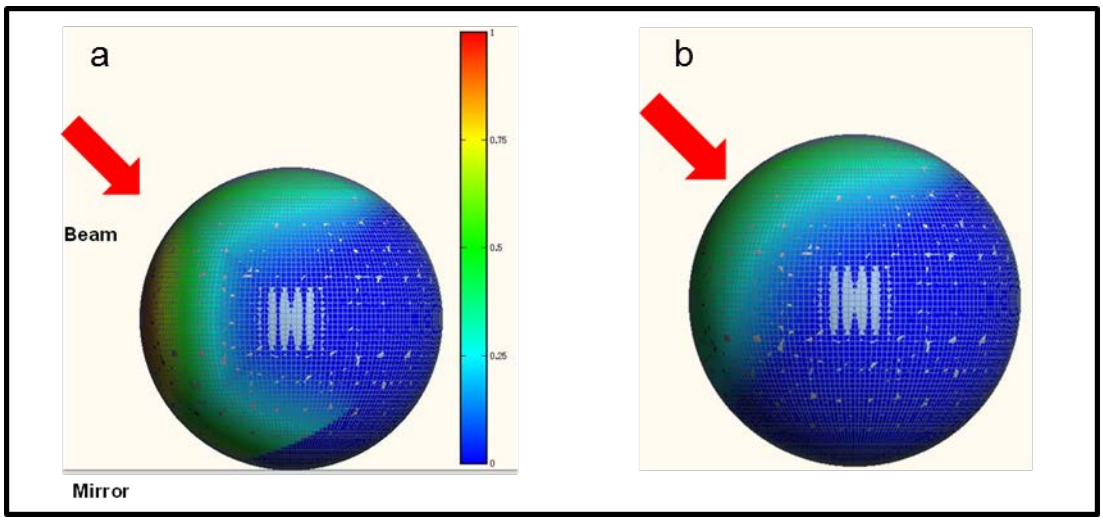

Figure 9: Schematics showing (a) distribution of absorbed laser light on the Ti particle surface and (b) expansion of the blowoff plasma, its burns of the mirror surface, and the recoil of the molten particle along the mirror surface.

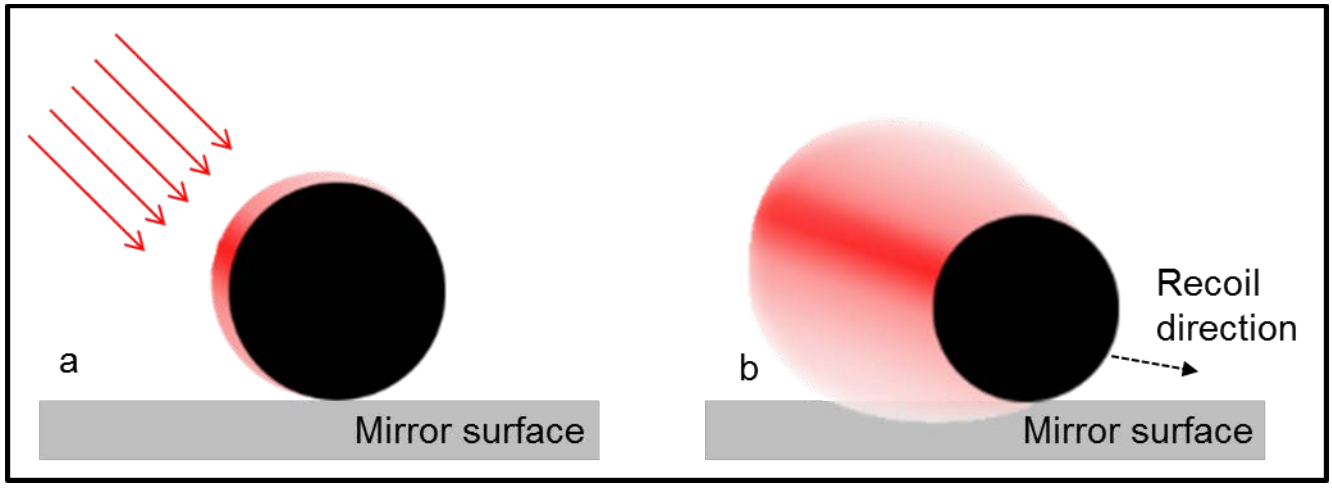

Table 1: Mechanical parameters for SiO_2, Al_2O_3, and HfO_2 thin coating films.

	E (GPa)	ν	$\alpha(1/K) \times 10^{6}$
SiO_2	73	0.17	0.55
Al_2O_3	300	0.21	8.1
HfO_2	260	0.3	3.6